THE JOURNAL OF BIOLOGICAL CHEMISTRY VOL. 288, NO. 22, pp. 15900–15912, May 31, 2013

Palmitoylation of Protease-activated Receptor-1 Regulates Adaptor Protein Complex-2 and -3 Interaction with Tyrosine-based Motifs and Endocytic Sorting*[S]

Received for publication, March 15, 2013 Published, JBC Papers in Press, April 11, 2013, DOI 10.1074/jbc.M113.469866

Isabel Canto[‡1] **and JoAnn Trejo**[§2]

From the [‡]*Biomedical Sciences Graduate Program and the* [§]*Department of Pharmacology, School of Medicine, University of California, San Diego, La Jolla, California 92093*

Background: Protease-activated receptor-1 (PAR1) trafficking is regulated by adaptor protein complex-2 and -3 interaction with C-tail tyrosine motifs.
Results: A palmitoylation-deficient PAR1 mutant displays altered utilization of tyrosine motifs and dysregulated trafficking.
Conclusion: Palmitoylation of PAR1 is necessary for proper adaptor protein recognition of tyrosine motifs and trafficking.
Significance: Defects in PAR1 palmitoylation cause dysregulated trafficking that likely abrogates expression at the cell surface.

Protease-activated receptor-1 (PAR1) is a G protein-coupled receptor for the coagulant protease thrombin. Thrombin binds to and cleaves the N terminus of PAR1, generating a new N terminus that functions as a tethered ligand that cannot diffuse away. In addition to rapid desensitization, PAR1 trafficking is critical for the regulation of cellular responses. PAR1 displays constitutive and agonist-induced internalization. Constitutive internalization of unactivated PAR1 is mediated by the clathrin adaptor protein complex-2 (AP-2), which binds to a distal tyrosine-based motif localized within the C-terminal tail (C-tail) domain. Once internalized, PAR1 is sorted from endosomes to lysosomes via AP-3 interaction with a second C-tail tyrosine motif proximal to the transmembrane domain. However, the regulatory processes that control adaptor protein recognition of PAR1 C-tail tyrosine-based motifs are not known. Here, we report that palmitoylation of PAR1 is critical for regulating proper utilization of tyrosine-based motifs and endocytic sorting. We show that PAR1 is basally palmitoylated at highly conserved C-tail cysteines. A palmitoylation-deficient PAR1 mutant is competent to signal and exhibits a marked increase in constitutive internalization and lysosomal degradation compared with wild type receptor. Intriguingly, enhanced constitutive internalization of PAR1 is mediated by AP-2 and requires the proximal tyrosine-based motif rather than the distal tyrosine motif used by wild type receptor. Moreover, palmitoylation-deficient PAR1 displays increased degradation that is mediated by AP-3. These findings suggest that palmitoylation of PAR1 regulates appropriate utilization of tyrosine-based motifs by adaptor proteins and endocytic trafficking, processes that are critical for maintaining appropriate expression of PAR1 at the cell surface.

In the event of vascular injury and in thrombotic disease, the coagulant protease thrombin is generated and elicits cellular responses through the activation of protease-activated receptor-1 (PAR1),[3] a G protein-coupled receptor (GPCR) (1, 2). PAR1 expression is essential for thrombin signaling in the vasculature and regulates platelet activation, endothelial cell activation, and embryonic development (3). PAR1 activation occurs through an unusual proteolytic mechanism. Thrombin binds to and cleaves the N terminus of PAR1, generating a new N-terminal domain that acts as a tethered ligand by binding intramolecularly to the receptor to initiate G protein signaling (4). Synthetic peptides that mimic the newly formed N terminus of PAR1 can activate the receptor independent of thrombin and receptor cleavage (4, 5). Activated PAR1 couples to multiple heterotrimeric G protein subtypes including G_q, $G_{i/o}$, and $G_{12/13}$ and promotes diverse cellular responses (1). Due to the irreversible proteolytic nature of activation, PAR1 signaling is tightly regulated through rapid desensitization and endocytic trafficking.

Similar to most classic GPCRs, activated PAR1 is rapidly desensitized by phosphorylation and β-arrestin binding (6, 7). In addition to desensitization, trafficking of PAR1 is critical for regulation of thrombin signaling (8, 9). PAR1 displays constitutive and agonist-induced internalization that occurs independent of β-arrestins (6). Constitutive internalization of PAR1 is mediated by the clathrin adaptor protein complex-2 (AP-2) (10), a heterotetrameric complex composed of α, β2, μ2, and σ adaptin subunits. AP-2 regulates internalization of transmembrane proteins via μ2-adaptin subunit interaction with tyrosine-based *YXX*$\varnothing$ motifs, where *Y* is tyrosine, *X* denotes any amino acid, and $\varnothing$ is a bulky hydrophobic residue (11, 12). PAR1 contains two tyrosine-based motifs within its C-terminal tail (C-tail) located proximal to the seventh transmembrane

* This work was supported, in whole or in part, by National Institutes of Health Grant GM090689 (to J. T.).
[S] This article contains supplemental Figs. 1.
[1] Supported by an University of California Tobacco-related Disease Research Program Dissertation Award 21DT-0096.
[2] To whom correspondence should be addressed: 9500 Gilman Dr., BSB Rm. 3044A, La Jolla, CA 92093. Tel.: 858-246-0150; Fax: 858-822-0041; E-mail: joanntrejo@ucsd.edu.

[3] The abbreviations used are: PAR1, protease-activated receptor-1; GPCR, G protein-coupled receptor; AP-2, adaptor protein complex-2; C-tail, C-terminal carboxyl tail; AP-3 adaptor protein complex-3; BRET, bioluminescence resonance energy transfer; EEA1, early endosomal antigen-1; Rluc, *R. reniformis* luciferase; LAMP1, lysosomal-associated membrane protein 1; ANOVA, analysis of variance; TP, thromboxane A2 receptor.

domain and at the distal end of the C-tail. We previously showed that the μ2-adaptin subunit of AP-2 binds directly to the PAR1 C-tail distal tyrosine-based motif to facilitate constitutive internalization and cellular resensitization (10, 13). After activation, PAR1 is internalized, sorted predominantly to lysosomes, and degraded, a process critical for termination of G protein signaling (14). In contrast to constitutive internalization, activated PAR1 internalization is dually regulated by the clathrin adaptors AP-2 and epsin-1, which recognize distinct C-tail phosphorylation and ubiquitination sorting signals (15). Once internalized, PAR1 is sorted from endosomes to lysosomes via AP-3 interaction with the proximal tyrosine motif (16, 17), a process that occurs independent of ubiquitination. Whether additional regulatory events control PAR1 sorting from endosomes to lysosomes is not known.

Posttranslational modifications are essential for the proper regulation of all GPCRs. In addition to phosphorylation, many GPCRs are modified by palmitoylation (18). Palmitoylation occurs through the covalent attachment of palmitate, a 16-carbon saturated fatty acid, to cysteine residues via a thioester linkage. This modification is a dynamic reversible process in which the palmitoyl group is added enzymatically through palmitoyl acyltransferases and removed by palmitoyl-protein thioesterases (19). Many, but not all, GPCRs are palmitoylated within the C-tail domain on juxtamembrane cysteine residues (20, 21). Defective GPCR palmitoylation has been shown to impair coupling to G proteins and to alter membrane trafficking (18). However, in most cases the molecular mechanisms responsible for GPCR dysfunction due to loss of palmitoylation are not known.

Given the importance of PAR1 regulatory processes for the fidelity of thrombin signaling, we sought to determine whether PAR1 is modified by palmitoylation and the function of such a posttranslational modification. In this study we demonstrate for the first time that PAR1 is palmitoylated on highly conserved C-tail cysteine residues. A palmitoylation-deficient PAR1 mutant is trafficked to the cell surface and competent to signal. However, the palmitoylation-deficient PAR1 mutant exhibited an enhanced rate of constitutive internalization and lysosomal degradation compared with wild type receptor. We further show that dysregulated trafficking of the palmitoylation-deficient PAR1 mutant is due to inappropriate utilization of tyrosine-based motifs by the AP-2 and AP-3 sorting complexes. These studies indicate that palmitoylation of PAR1 is critical for regulating proper trafficking through the endocytic system, and defects in palmitoylation result in inappropriate PAR1 internalization from the cell surface and subsequent degradation.

EXPERIMENTAL PROCEDURES

Reagents and Antibodies—PAR1 peptide agonist SFLLRN was synthesized as the carboxyl amide and purified by reverse-phase high pressure liquid chromatography at Tufts University Core Facility (Boston, MA). Human α-thrombin was obtained from Enzyme Research Laboratories (South Bend, IN). Rabbit polyclonal anti-FLAG antibody, mouse monoclonal M1 and M2 anti-FLAG antibodies, and mouse monoclonal anti-β-actin were purchased from Sigma. Anti-early endosomal antigen-1 (EEA1) antibody, anti-μ2 adaptin AP-50, and anti-δ-subunit AP-3 antibody were obtained from BD Biosciences. Lysosomal-associated membrane protein 1 (LAMP1) antibody was obtained from the Developmental Studies Hybridoma Bank (University of Iowa, Iowa City, IA). The anti-PAR1 WEDE mouse antibody was from Beckman Coulter (Fullerton, CA). The anti-PAR1 C5433 rabbit polyclonal antibody was previously described (10). Horseradish peroxidase (HRP)-conjugated secondary goat anti-mouse and goat anti-rabbit antibodies were from Bio-Rad. Alexa Fluor® 488- and 594-conjugated goat anti-mouse and anti-rabbit antibodies were obtained from Invitrogen. De-lipidated fetal bovine serum was obtained from Omega Scientific (Tarzana, CA).

cDNAs and Cell Lines—A cDNA plasmid encoding an N-terminal FLAG-tagged human PAR1 and tyrosine-based motif mutants cloned into pBJ vector were previously described (10, 22). A PAR1 mutant in which cysteine (Cys) residues at positions 387 and 388 were mutated to alanines (Ala) was generated by QuikChange site-directed mutagenesis (Agilent Technologies, Santa Clara, CA). A PAR1 wild type (WT) fused to yellow fluorescent protein (YFP) cloned into pRK6 vector was generously provided by Dr. Jean-Philippe Pin (Montpellier University). The PAR1 CC/AA-YFP mutant was generated by QuikChange site-directed mutagenesis. A plasmid encoding μ2-adaptin with a C-terminal *Renilla reniformis* luciferase (Rluc) cloned into pcDNA3 was generated using standard subcloning techniques. All cDNA plasmids were subjected to dideoxy sequencing (Retrogen, San Diego, CA). HeLa cells stably expressing FLAG-tagged PAR1 CC/AA mutant were generated and maintained as previously described (22). Human umbilical vein endothelial-derived EA.hy926 cells were maintained as described (23).

Cell Transfections—HeLa cells were transiently transfected with FLAG-PAR1 WT and mutants using Lipofectamine 2000 (Invitrogen), polyethyleneimine (Polysciences, Warrington PA), or JetPrime (Polyplus Transfection Inc., New York NY) reagents according to the manufacturer's instructions. COS7 cells were transiently transfected with PAR1 WT-YFP or PAR1 CC/AA-YFP and μ2-Rluc using FuGENE 6 (Promega, Madison WI). HeLa cells were transiently transfected with nonspecific, μ2-adaptin, or δ-adaptin siRNAs using Oligofectamine (Invitrogen) or JetPrime according to the manufacturer's instructions. The nonspecific siRNA 5′-CTACGTCCAGGAGCGCACC-3′ and μ2 siRNA 5′-GTGGATGCCTTTCGGGTCA-3′ were synthesized by Thermo Scientific Dharmacon Inc. (Lafayette, CO). The δ-adaptin SMARTpool siRNAs were purchased from Dharmacon Inc.

Immunoblotting—Equivalent amounts of cell lysates were resolved by SDS-PAGE, transferred to membranes, and immunoblotted with appropriate antibodies.

PAR1 Palmitoylation—Palmitoylation of PAR1 was examined in EA.hy926 and HeLa cells. HeLa cells were seeded at 2.5×10^5 cells/well in 6-well plates and transfected with PAR1 WT or CC/AA mutant. EA.hy926 cells were seeded at 1.5×10^6 cells per 10-cm^2 dish. Cells were grown in Dulbecco's modified Eagle's medium (DMEM) supplemented with 10% de-lipidated fetal bovine serum overnight and then incubated with 500 μCi/ml [^{3}H]palmitic acid (PerkinElmer Life Sciences) for 3 h in

10% de-lipidated serum/DMEM. Cells were serum-starved for 1 h and then left untreated or treated with agonist for various times at 37 °C. Cells were lysed in buffer containing 1% Triton X-100, 50 mM Tris-HCl, pH 7.4, 100 mM NaCl, 5 mM EDTA, 50 mM NaF, and 10 mM sodium pyrophosphate supplemented with protease inhibitors 100 μg/ml PMSF, 1 μg/ml leupeptin, 2 μg/ml aprotinin, 1 μg/ml pepstatin A, 10 μg/ml benzamidine, and 1 μg/ml soybean trypsin inhibitor. Total cell lysates were immunoprecipitated with either M2 anti-FLAG or anti-PAR1 WEDE antibody overnight at 4 °C. Immunoprecipitates were resolved on 9% SDS-PAGE, and gels were fixed with a 25% isopropyl alcohol, 10% glacial acetic acid solution then incubated for 30 min in NAMP100 (GE Healthcare) or fixed with a 10% glacial acetic acid, 30% methanol solution and then incubated with En^{3}Hance (PerkinElmer Life Sciences). Gels were dried and exposed to Amersham Biosciences Hyperfilm (GE Healthcare) with intensifying screens at −80 °C. Aliquots of immunoprecipitates were also resolved by SDS-PAGE, transferred to membranes, and immunoblotted to detect PAR1 expression.

Immunofluorescence Confocal Microscopy—HeLa cells expressing FLAG-PAR1 WT or mutants were prelabeled with anti-FLAG polyclonal antibody for 1 h at 4 °C and incubated in media at 37 °C for various times. Cells were fixed, permeabilized, and immunostained with anti-EEA1 or anti-LAMP1 antibodies followed by species-specific secondary antibodies conjugated to Alexa Fluor® 488 or 594 and imaged by confocal microscopy as described (17). Images were acquired using an Olympus DSU spinning disk confocal microscope configured with a PlanApo 60× oil objective and Hamamatsu ORCA-ER digital camera. Fluorescent images of *X-Y* sections at 0.28 μm were collected using Intelligent Imaging Innovations Slidebook 4.2 Software (Denver, CO). The final composite images were created using Adobe Illustrator CS5 (San Jose, CA). Pearson's correlation coefficients (*r*) were determined using SlideBook 4.2 software and derived from an algorithm that provides a quantifiable analysis of degree of overlap based on pixel intensity of red and green fluorescence signals. A value of 1 indicates that fluorescent signals are perfectly correlated, whereas a value of 0 indicates that the signals are uncorrelated (24).

Antibody Uptake ELISA—The internalization of PAR1 was assessed by examining the uptake of antibody bound to PAR1 using a sandwich ELISA as previously described (25, 26). Briefly, HeLa cells stably expressing FLAG-PAR1 WT or CC/AA mutant were seeded at 1.0×10^5 cells/well in 24-well plates and grown overnight. Cells were serum-starved, labeled with M1 anti-FLAG antibody for 1 h at 4 °C, washed, and then incubated in media with or without agonist for varying times at 37 °C. Remaining surface-bound antibody was stripped with 1 mM EDTA-PBS at 4 °C. Cells were lysed and processed using a sandwich ELISA and the HRP substrate 1 Step 2,2′-azino-bis-3-ethylbenzthiazoline-6-sulfonic acid (ABTS) (Thermo Fisher, Rockford, IL) as described (25, 26). After 20 min the optical density of an aliquot was measured at 405 nm using a Molecular Devices SpectraMax Plus spectrophotometer (Sunnyvale, CA).

Cell Surface ELISA—HeLa cells expressing FLAG-PAR1 WT or CC/AA mutant were seeded at 1.0×10^5 cells/well in 24-well plates and grown overnight. Cells were fixed with 4% paraformaldehyde for 5 min at 4 °C, incubated with anti-FLAG polyclonal antibody and then with goat anti-rabbit HRP-conjugated secondary antibody for 1 h at room temperature, and developed as described above. The internalization of PAR1 was measured as described (27). Briefly, HeLa cells seeded 0.8×10^5 cells/well in 24-well plates transfected with FLAG-PAR1 WT or various mutants were labeled with M1 anti-FLAG antibody at 4 °C, washed, and incubated in DMEM containing 0.1% BSA, 20 mM HEPES, 1 mM Ca^{2+} at 37 °C. After internalization, cells were fixed and processed as described above.

Phosphoinositide Hydrolysis—HeLa cells were seeded at 0.75×10^5 cells/well in 24-well plates and transfected with FLAG-PAR1 WT, CC/AA mutant, or pBJ vector control. Cells were then labeled with 1.0 μCi/ml *myo*-[^{3}H]inositol (American Radiolabeled Chemicals, St. Louis, MO) in inositol-free DMEM overnight, washed, and stimulated with thrombin in the presence of 20 mM LiCl for various times at 37 °C. The amounts of accumulated [^{3}H]inositol phosphates were measured as described (6).

PAR1 Degradation Assays—HeLa cells seeded in 24-well plates were transiently transfected with FLAG-PAR1 WT or CC/AA mutant. Cells were serum-starved and then incubated with 10 μM cycloheximide for various times and lysed in 2× SDS sample buffer containing 125 mM Tris-HCl at pH 6.8, 20% v/v glycerol, 10% w/v SDS, 0.02% w/v bromphenol blue. Cell lysates were resolved by SDS-PAGE, transferred to membranes, and immunoblotted with polyclonal anti-FLAG antibody.

BRET Assays—COS7 cells were seeded at 2.5×10^5 cells/well in 6-well plates. Cells were transfected with 100 ng of β2-adaptin Rluc and varying amounts of PAR1 WT-YFP or CC/AA-YFP mutant. Serum-starved cells were washed, dissociated using a non-enzymatic solution Cellstripper™ (Mediatech Inc.), resuspended in PBS containing 0.5 mM $MgCl_2$ and 0.1% glucose, and counted. Cells (~4×10^4 in 80 μl) were transferred to 96-well plates in triplicate for each condition. The fluorescence intensity of YFP was examined by excitation at 485 nm and emission at 535 nm using a Berthold Tristar LB 941 microplate reader (Berthold Technologies, GmbH and Co.). The coelenterazine H (Biotium Inc.) substrate was added to cells at a final concentration of 5 μM. After an 8-min delay, Rluc and YFP signals were determined using 480 and 530 nm filters, respectively. The BRET ratio was calculated as (emission at 530 nm)/(emission at 480 nm), and net BRET signal was determined by subtracting the background BRET, which is the BRET ratio from cells expressing Rluc construct only. Total luminescence was measured by integrating the signal for 1 s/well without filter selection. Data were fitted with non-linear regression using GraphPad Prism 4.0 software (GraphPad Inc., La Jolla, CA).

PAR1 Biotinylation Assays—HeLa cells were seeded in 6-well plates and transfected with FLAG PAR1 WT or CC/AA mutant. Serum-starved cells were labeled with 0.3 mg/ml EZ-link Sulfo-NHS-SS-biotin (Thermo Fisher) in PBS, pH 8.0, for 30 min on ice. Unbound biotin was quenched with 50 mM Tris HCl, pH 7.5, 275 mM NaCl, 6 mM KCl, and 2 mM $CaCl_2$, and cells were either left on ice or warmed to 37 °C. To remove the biotin label from the cell surface, cells were incubated with 50 mM glutathione, 75 mM NaCl, 75 mM NaOH, 1% BSA in PBS, pH 8.7,

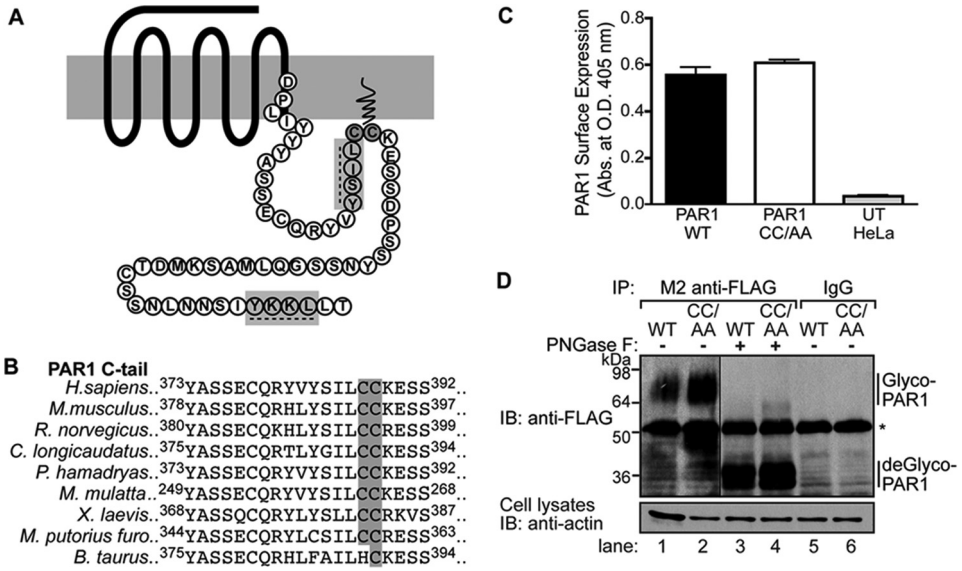

FIGURE 1. **PAR1 CC/AA mutant is expressed on the cell surface and glycosylated.** *A*, shown is a Snake diagram of the human PAR1 C-tail starting from the DP*XXY* motif. The cysteine site(s) of palmitoylation is *highlighted in gray*. Tyrosine-based sorting motifs are indicated with a *dashed line* and *highlighted in gray*. *B*, sequence alignment of PAR1 C-tail sequences from nine different species is shown. The conserved cysteines are *highlighted in gray*. Superscripted numbers indicate the position of amino acids. *C*, surface expression of FLAG-PAR1 WT or CC/AA mutant in HeLa cells compared with untransfected (*UT*) cells was quantified by ELISA. Data (mean ± S.D.) are representative of three independent experiments. *D*, HeLa cells expressing FLAG-PAR1 WT or CC/AA mutant were immunoprecipitated (*IP*) with M2 anti-FLAG antibody or IgG control. Immunoprecipitates were treated with or without peptide *N*-glycosidase F (*PNGase F*) for 1 h at 37 °C, resolved by SDS-PAGE, and immunoblotted (*IB*) with rabbit polyclonal anti-FLAG antibody to detect PAR1. *Glyco-PAR1* indicates the fully glycosylated PAR1, and *deGlyco-PAR1* indicates the deglycosylated receptor after peptide *N*-glycosidase F treatment. The *asterisk* indicates a nonspecific band detected by the anti-FLAG antibody. Cell lysates were immunoblotted for actin as a loading control.

for 10 min on ice, with gentle agitation, three times. Cells were washed three more times with PBS, pH 7.4, before further incubation at 37 °C. Cells were lysed in buffer containing 50 mM Tris HCl, pH 7.4, 250 mM NaCl, 5 mM EDTA, and 0.5% Triton X-100 supplemented with protease inhibitors as described above. Equivalent amounts of lysates were incubated with streptavidin-conjugated-agarose beads (Thermo Fisher) overnight at 4 °C and then washed 3 times with lysis buffer, eluted with 2× SDS sample buffer containing 0.2 M DTT, resolved by SDS-PAGE, and immunoblotted to detect PAR1.

Data Analysis—The data were analyzed using GraphPad Prism 4.0 software. Statistical analysis was determined by performing one-way ANOVA and Dunnett's post hoc test or two-way ANOVA and the Bonferroni post hoc test.

RESULTS

Palmitoylation of PAR1—PAR1 has not been shown to be palmitoylated, although previous studies have predicted PAR1 palmitoylation to occur at C-tail cysteine residues near the seventh transmembrane domain based on molecular modeling comparisons with rhodopsin (Fig. 1*A*) (28). Currently, there is no known consensus sequence for palmitoylation; therefore, we used NCBI basic local alignment search tool (BLAST) to align C-tail sequences from 30 different PAR1 species (supplemental Fig. S1). We identified two highly conserved cysteine residues at positions 387 and 388 of the human protein; both were present in 24 different species and could serve as potential sites for palmitoylation (Fig. 1*B* and supplemental Fig. S1). To determine whether these sites are targeted for palmitoylation, a PAR1 mutant was created in which Cys-387 and -388 were converted to alanines and is designated PAR1 CC/AA. HeLa cells stably expressing FLAG-tagged PAR1 WT and the CC/AA mutant were generated to facilitate the characterization of receptor palmitoylation. Both FLAG-PAR1 WT and CC/AA mutant were expressed at the cell surface as assessed by ELISA (Fig. 1*C*). In addition, immunoprecipitated FLAG-PAR1 WT and CC/AA mutant migrated as prominent species between ~64 and 98 kDa (Fig. 1*D*, *lanes 1* and *2*) and were not detected in IgG immunoprecipitates (Fig. 1*D*, *lanes 5* and *6*). Incubation of PAR1 WT and CC/AA mutant with the endoglycosidase peptide *N*-glycosidase F (*PNGase F*) resulted in a size shift to ~36 kDa (Fig. 1*D*, *lanes 3* and *4*), consistent with the predicted molecular mass of unmodified human PAR1. These findings suggest that the PAR1 CC/AA mutant is glycosylated and trafficked to the cell surface similar to wild type receptor.

To determine whether PAR1 is modified by palmitoylation, we directly measured [^{3}H]palmitate incorporation during metabolic labeling. HeLa cells expressing FLAG-PAR1 WT or CC/AA mutant labeled with [^{3}H]palmitate were incubated in the absence or presence of agonist peptide SFLLRN for various times at 37 °C. Cells were lysed, and PAR1 was immunoprecipitated, resolved by SDS-PAGE, and then subjected to fluorography. In untreated control cells, wild type PAR1 labeled with [^{3}H]palmitate migrated as a major species between ~50 and 75 kDa (Fig. 2*A*, *lane 1*), consistent with the fully glycosylated PAR1 (Fig. 1*D*, *lane 1*). The amount of [^{3}H]palmitate incorporated into PAR1 WT was unchanged after 3 or 10 min of agonist stimulation compared with untreated control cells (Fig. 2*A*, *lanes 1–3*). In contrast to wild type receptor, the PAR1 CC/AA mutant failed to incorporate [^{3}H]palmitate under control or agonist-stimulated conditions (Fig. 2*A*, *lanes 4* and *5*). Endogenous PAR1 expressed in human endothelial cells also exhibited basal palmitoylation that was not substantially altered after

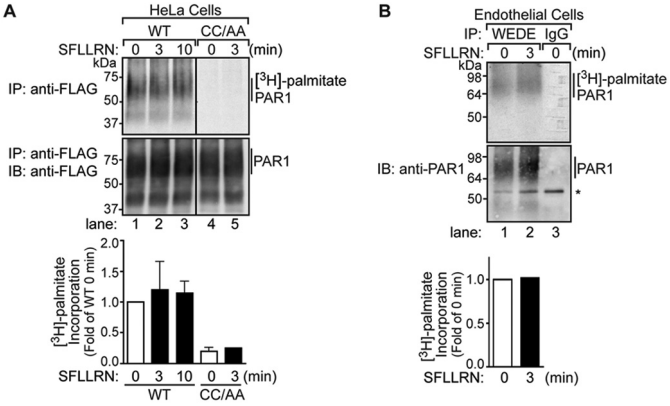

FIGURE 2. **PAR1 is posttranslationally modified by palmitoylation.** *A*, HeLa cells expressing FLAG-PAR1 WT or CC/AA mutant were labeled with [^{3}H]palmitic acid and left untreated or treated with 100 μM SFLLRN for various times at 37 °C. Cells were lysed and processed, and PAR1 was immunoprecipitated (*IP*) with M2 anti-FLAG antibody. Immunoprecipitates were resolved by SDS-PAGE and processed for fluorography to detect [^{3}H]palmitate or immunoblotted (*IB*) with polyclonal anti-FLAG antibody to detect receptor. Three independent experiments were quantified, and the amount [^{3}H]palmitate incorporation, normalized to receptor in immunoprecipitates, was determined. The data shown (mean ± S.D.; $n = 3$) are expressed as -fold wild type PAR1 0 min control. *B*, human cultured endothelial EA.hy926 cells labeled with [^{3}H]palmitic acid were stimulated with 100 μM SFLLRN for 3 min at 37 °C. Cells were lysed and immunoprecipitated with anti-PAR1 WEDE antibody and processed as described above. The *asterisk* indicates a nonspecific band. The incorporation of [^{3}H]palmitate was quantified, normalized to receptor in immunoprecipitates, and is expressed as -fold increase over untreated 0 min control.

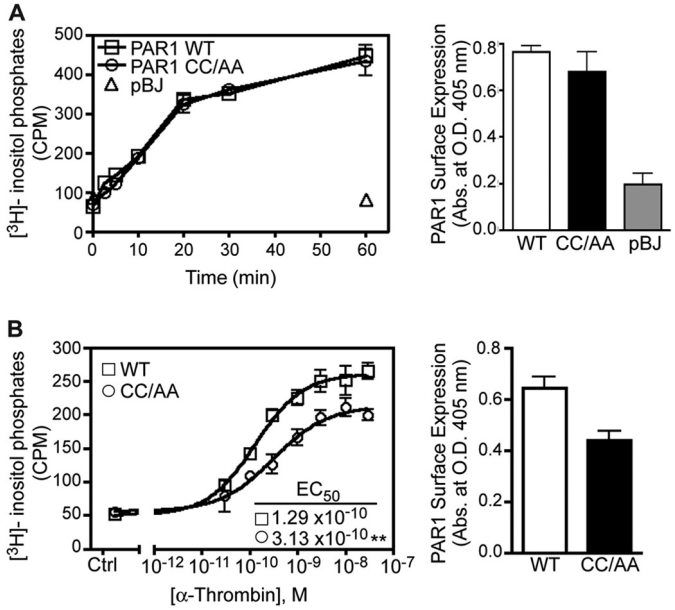

FIGURE 3. **Signaling by the palmitoylation-deficient PAR1 mutant.** *A*, HeLa cells transfected with FLAG-PAR1 WT, CC/AA mutant, or pBJ vector were labeled with *myo*-[^{3}H]inositol and stimulated with 10 nM α-thrombin for various times at 37 °C. The data (mean ± S.D.; $n = 3$) represent the accumulation of [^{3}H]inositol phosphates in counts per min (cpm). Cell surface expression of PAR1 WT-, CC/AA-, and pBJ-transfected cells from the same experiment was determined by ELISA (mean ± S.D.; $n = 3$). *B*, HeLa cells transfected with FLAG-PAR1 WT or CC/AA mutant labeled with *myo*-[^{3}H]inositol were treated with varying concentrations α-thrombin for 20 min at 37 °C. The data (mean ± S.D.; $n = 3$) represent the accumulation of [^{3}H]inositol phosphates expressed as cpm. The EC_{50} values calculated for PAR1 WT (1.29×10^{-10} M) *versus* CC/AA mutant (3.13×10^{-10} M) were statistically significantly different (**, $p < 0.01$). Cell surface expression of PAR1 WT and CC/AA mutant from the same experiment was determined by ELISA (mean ± S.D.; $n = 3$).

incubation with agonist (Fig. 2*B*, *lanes 1* and *2*). These observations suggest that PAR1 is basally palmitoylated at C-tail Cys-387 and -388 residues. However, the metabolic labeling conditions employed in these assays cannot distinguish if PAR1 is dynamically palmitoylated and de-palmitoylated at steady state.

Palmitoylation-deficient PAR1 Mutant Signaling—To assess the function of PAR1 palmitoylation, we first compared the signaling properties of PAR1 WT *versus* CC/AA mutant. Activation of PAR1 is known to couple to phospholipase C-mediated phosphoinositide hydrolysis, a response attributed mainly to G_q coupling (29, 30). HeLa cells expressing similar amounts of PAR1 WT and CC/AA mutant on the cell surface (Fig. 3*A*) were labeled with *myo*-[^{3}H]inositol and incubated with 10 nM thrombin for various times at 37 °C, and [^{3}H]inositol phosphates formed were quantified as previously described (7). Thrombin-activation of PAR1 WT and CC/AA mutant resulted in a similar initial rapid increase in phosphoinositide hydrolysis followed by a slower sustained phase of [^{3}H]inositol phosphate generation after 20 min, and maximal [^{3}H]inositol phosphate accumulation was detected at 60 min (Fig. 3*A*). No change in [^{3}H]inositol phosphate accumulation was detected in pBJ vector-transfected cells treated with thrombin for 60 min (Fig. 3*A*), indicating that thrombin signaling is PAR1-dependent. We next evaluated the coupling of PAR1 WT and CC/AA mutant to G protein-stimulated signaling by examining the concentration effect curve of thrombin-induced phosphoinositide hydrolysis (Fig. 3*B*). HeLa cells expressing PAR1 WT and CC/AA mutant labeled with *myo*-[^{3}H]inositol were treated with varying concentrations of thrombin for 20 min at 37 °C, and the generation of [^{3}H]inositol phosphates was measured. The effective concentration of thrombin needed to stimulate half-maximal response (EC_{50}) for PAR1 WT *versus* CC/AA mutant was significantly different (Fig. 3*B*), suggesting that palmitoylation regulates receptor coupling to G_q-stimulated signaling. These results are consistent with a previous report that employed a PAR1 mutant containing Cys-387 and -388 to serine (Ser) mutations (28), although palmitoylation of PAR1 was not examined in the study. Together these findings suggest that although palmitoylation is not essential for PAR1 signaling, it can modulate receptor-G protein coupling.

Palmitoylation-deficient PAR1 Mutant Displays Enhanced Constitutive Internalization—The trafficking behavior of palmitoylation-deficient PAR1 was examined to further characterize the function of palmitoylation. To assess constitutive internalization, FLAG-PAR1 WT and CC/AA mutant expressed in HeLa cells were labeled with M1 anti-FLAG antibody for 1 h at 4 °C to ensure only receptors at the cell surface bound antibody. Unbound antibody was removed by washing, and constitutive internalization of PAR1 was determined after incubation for various times at 37 °C by ELISA as we previously described (26). After a 30-min incubation, ~10% of PAR1 WT was detected in an intracellular compartment (Fig. 4*A*), which is consistent with the extent of wild type receptor constitutive internalization previously reported in these cells (26). In contrast, PAR1 CC/AA mutant exhibited enhanced constitutive internalization with ~30% receptor accumulation measured at 30 min (Fig. 4*A*). However, agonist-induced PAR1 WT

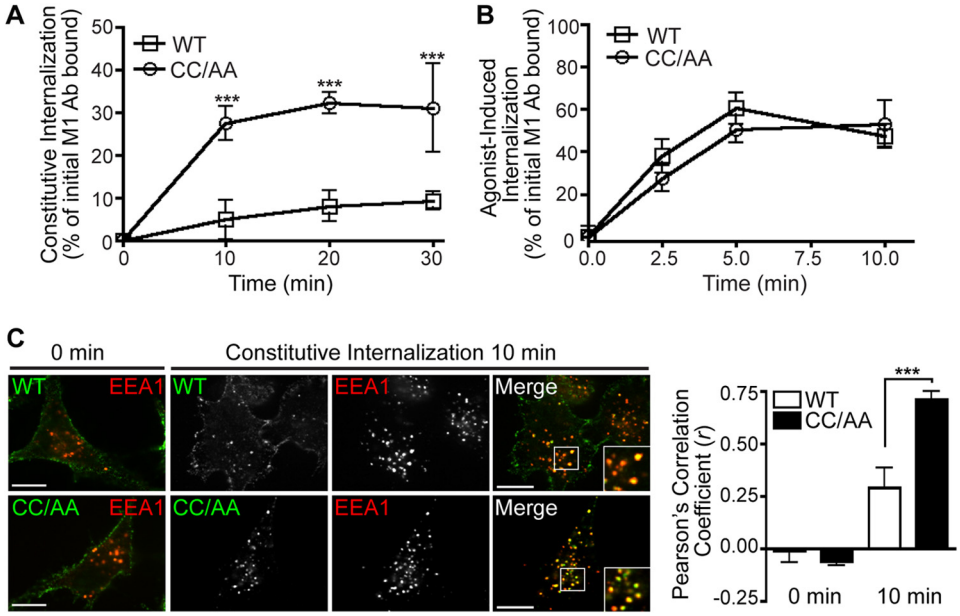

FIGURE 4. **Palmitoylation-deficient PAR1 displays enhanced constitutive internalization.** *A*, HeLa cells expressing FLAG-PAR1 WT or CC/AA mutant were prelabeled with M1 anti-FLAG at 4 °C, then incubated in media without agonist for various times at 37 °C. Internalized receptor bound antibody (*Ab*) was quantified by sandwich ELISA. Data shown (mean ± S.D.; $n = 3$) are expressed as a percentage of the initial receptor-bound M1 antibody and are the average of three separate experiments performed in triplicate. Differences in constitutive internalization between PAR1 WT and CC/AA mutant were significant (***, $p < 0.001$) as determined by two-way ANOVA and Bonferroni post-tests. *B*, HeLa cells stably expressing FLAG-PAR1 WT or CC/AA mutant were incubated with 100 μM SFLLRN peptide agonist for various times 37 °C, and internalization was quantified as described above. Data shown (mean ± S.D.; $n = 3$) are expressed as a percentage of the initial receptor-bound M1 antibody and are representative of three individual experiments performed in triplicate. *C*, HeLa cells expressing FLAG-PAR1 WT or CC/AA were prelabeled with polyclonal anti-FLAG antibody at 4 °C, then incubated for 30 min at 37 °C. Cells were fixed, permeabilized, and co-stained for endogenous EEA1 and imaged by confocal microscopy. *Insets* are magnifications of the *boxed areas*. Images are representative of many cells examined in multiple independent experiments. Colocalization of PAR1 (*green*) and EEA1 (*red*) is indicated by the *yellow* color in the merged images and was quantified by determining Pearson's correlation coefficients (*r*) from seven different cells. The difference in PAR1 CC/AA *versus* WT colocalization with EEA1 at 10 min was statistically significant (***, $p < 0.001$) as determined by a Student's *t* test. *Scale bar*, 10 μm.

and CC/AA mutant internalization was comparable (Fig. 4*B*). Immunofluorescence confocal microscopy confirmed enhanced constitutive internalization of the palmitoylation-deficient PAR1 mutant. HeLa cells expressing PAR1 WT or CC/AA mutant were labeled with antibody at 4 °C and fixed (0 min) or incubated at 37 °C for 10 min and then fixed, permeabilized, and co-stained for EEA1, a marker of early endosomes (Fig. 4*C*). Both PAR1 WT and CC/AA mutant localized to the cell surface at 0 min (Fig. 4*C*). However, after a 10-min incubation at 37 °C, a greater number of EEA1-positive puncta containing PAR1 CC/AA mutant was evident compared with wild type receptor (Fig. 4*C*), consistent with enhanced constitutive internalization. The difference in PAR1 CC/AA mutant colocalization with EEA1 compared with wild type receptor was verified by determining Pearson's correlation coefficients (Fig. 4*C*). These results suggest that palmitoylation is important for regulatory processes that control PAR1 constitutive internalization.

AP-2 Mediates Constitutive Internalization of Palmitoylation-deficient PAR1—To examine the function of AP-2 in constitutive internalization of the palmitoylation-deficient PAR1 mutant, we first examined whether AP-2 interacted with the receptor in living cells using BRET. BRET was assessed in COS7 cells transfected with a constant amount of the μ2-adaptin fused to Rluc together with varying amounts of PAR1 WT or CC/AA mutant tagged with YFP at the C terminus. A hyperbolic increase in BRET was detected as the ratio of PAR1 WT-YFP or CC/AA-YFP to μ2-adaptin Rluc was increased, suggesting that receptor-μ2-adaptin protein interaction is specific (Fig. 5*A*). To evaluate the relative affinity of PAR1 WT *versus* CC/AA mutant to AP-2, the $BRET_{50}$ values were determined and were not significantly different (Fig. 5*A*). However, the maximum BRET signal observed with PAR1 CC/AA-YFP and μ2-adaptin Rluc was greater than that exhibited by PAR1 WT-YFP and μ2-adaptin Rluc. These data suggest that PAR1 CC/AA mutant binds to AP-2 with a similar affinity as wild type PAR1, but the interaction is likely different.

To further investigate AP-2 function, we examined whether constitutive internalization of palmitoylation-deficient PAR1 is AP-2-dependent, like that shown for the wild type receptor (10). HeLa cells expressing similar amounts of FLAG-PAR1 WT or CC/AA mutant on the cell surface were transiently transfected with nonspecific siRNAs or siRNAs targeting the μ2-adaptin subunit, which disrupt AP-2 function. Cells transfected with μ2-adaptin subunit siRNA exhibited a marked decrease in μ2-adaptin expression compared with nonspecific control-transfected cells (Fig. 5*B*). As expected, PAR1 WT constitutive internalization was inhibited in cells lacking AP-2 expression compared with nonspecific siRNA-transfected control cells assessed after a 15-min incubation at 37 °C (Fig. 5*C*), consistent with previous reports (10). PAR1 CC/AA mutant exhibited enhanced constitutive internalization compared with wild type receptor in control siRNA-transfected cells, which was virtually ablated in AP-2-deficient cells (Fig. 5*C*). Immunofluorescence confocal microscopy confirmed that AP-2 mediates constitutive internalization of PAR1 WT or CC/AA

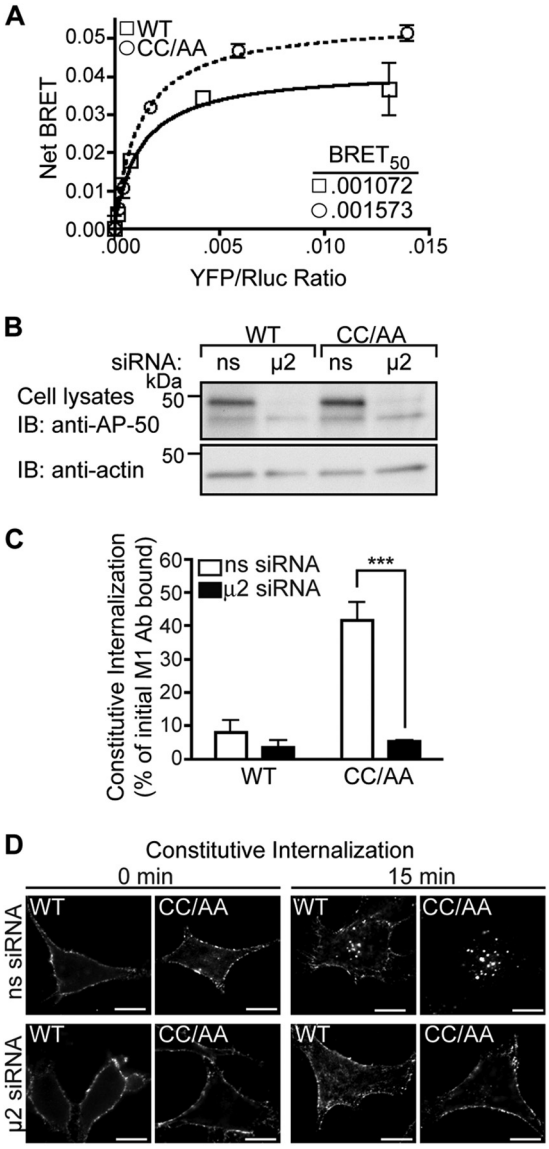

FIGURE 5. **AP-2 mediates enhanced constitutive internalization of palmitoylation-deficient PAR1.** *A*, COS7 cells were co-transfected with a fixed amount of μ2-adaptin fused to Rluc, and varying amounts of PAR1 WT-YFP or CC/AA-YFP and receptor-μ2 interaction was assessed by BRET. The data (mean ± S.D.; $n = 3$) shown are representative of three individual experiments. The *inset* shows $BRET_{50}$ values for PAR1 WT and CC/AA mutant. *B*, HeLa cells expressing FLAG-PAR1 WT or CC/AA mutant were transfected with siRNA targeting the μ2-adaptin subunit of AP-2 or nonspecific (*ns*) siRNA control. Cell lysates were immunoblotted (*IB*) for μ2-adaptin expression, and membranes were stripped and reprobed for actin. *C*, cells expressing FLAG-PAR1 WT or CC/AA mutant were serum-starved, prelabeled with M1 anti-FLAG antibody, and then incubated for 15 min at 37 °C. Internalized receptor-bound antibody was quantified by sandwich ELISA. Data shown (mean ± S.D.; $n = 3$) are expressed as a percentage of the initial receptor-bound M1 antibody and are representative of three separate experiments performed in triplicate. PAR1 CC/AA mutant constitutive internalization in ns-siRNA *versus* μ2-siRNA-transfected cells was significantly different (***, $p < 0.001$) as determined by two-way ANOVA and Bonferroni post-tests. *D*, HeLa cells expressing FLAG-PAR1 WT or CC/AA mutant were prelabeled with polyclonal anti-FLAG antibody and then incubated for 15 min at 37 °C. Cells were fixed, permeabilized, and immunostained for PAR1 and imaged by confocal microscopy. *Scale bar*, 10 μm.

mutant. HeLa cells expressing FLAG-PAR1 WT and CC/AA mutant transfected with siRNAs were prelabeled with anti-FLAG antibody, incubated at 37 °C for 15 min, fixed, and processed for microscopy. In nonspecific siRNA-transfected cells, PAR1 WT and CC/AA mutant localized to endocytic vesicles (Fig. 5*D*), whereas the receptors failed to internalize in cells deficient in AP-2 expression (Fig. 5*D*). These findings suggest that AP-2 regulates constitutive internalization of palmitoylation-deficient PAR1.

Palmitoylation of PAR1 Regulates Proper Utilization of C-tail YXX∅ Motifs—The PAR1 C-tail domain contains two tyrosine-based *YXX∅* sorting motifs that conform to canonical AP-2 binding sites (Fig. 6*A*) (11). We previously showed that the μ2-adaptin subunit of AP-2 binds directly to the distal tyrosine YKKL motif to mediate PAR1 constitutive internalization (10). To further define the function of AP-2 in enhanced PAR1 constitutive internalization, we generated receptor CC/AA variants harboring mutations in the proximal and distal tyrosine-based motifs (Fig. 6*A*). HeLa cells expressing FLAG-PAR1 wild type and mutants labeled with anti-FLAG antibody were incubated at 37 °C for 30 min, and constitutive internalization was examined by confocal microscopy and cell surface ELISA. The PAR1 CC/AA mutant exhibited a marked increase in internalization compared with wild type receptor as assessed by examining receptor-positive vesicles that colocalized with EEA1 using confocal microscopy (Fig. 6*B*). Enhanced PAR1 CC/AA mutant constitutive internalization was confirmed by quantifying the amount of receptor remaining at the cell surface by ELISA (Fig. 6*C*). As expected, the PAR1 AKKAA mutant failed to internalize (Fig. 6, *D* and *E*), consistent with a critical role for the distal tyrosine motif in mediating AP-2 binding and constitutive internalization of wild type receptor (10). Remarkably, however, mutation of the distal tyrosine motif of the palmitoylation-deficient PAR1 CC/AA mutant failed to inhibit constitutive internalization (Fig. 6, *D* and *E*). These findings suggest that in the absence of palmitoylation, the PAR1 distal tyrosine motif is no longer required for constitutive internalization, although PAR1 CC/AA+AKKAA constitutive internalization remains AP-2-dependent (Fig. 7*A*). We next examined the function of the PAR1 proximal tyrosine YSIL motif. Consistent with previous findings (10), PAR1 ASIA mutant exhibited a modest level of constitutive internalization that was comparable with wild type receptor (Fig. 6, *F* and *G*). In striking contrast, however, the palmitoylation-deficient PAR1 CC/AA mutant in which the proximal tyrosine motif was mutated to ASIA displayed impaired internalization (Fig. 6, *F* and *G*), suggesting that the proximal motif is now critical for constitutive internalization in the absence of palmitoylation. A small amount of PAR1 CC/AA+ASIA constitutive internalization was detected by immunofluorescence microscopy (Fig. 6*F*) but was completely abolished in AP-2-deficient cells (Fig. 7*B*). In addition, constitutive internalization of PAR1 CC/AA + ASIA mutant containing a defective distal motif AKKAA was virtually ablated (Fig. 6, *H* and *I*). Together these findings indicate that palmitoylation of PAR1 is important for proper utilization of C-tail tyrosine-based sorting motifs and regulation of receptor constitutive internalization.

Palmitoylation-deficient PAR1 Mutant Exhibits Enhanced Degradation—We recently showed that sorting of internalized PAR1 from early endosomes to lysosomes is mediated by AP-3 interaction with the receptor C-tail proximal tyrosine YSIL motif (16). Given the importance of PAR1 palmitoylation in

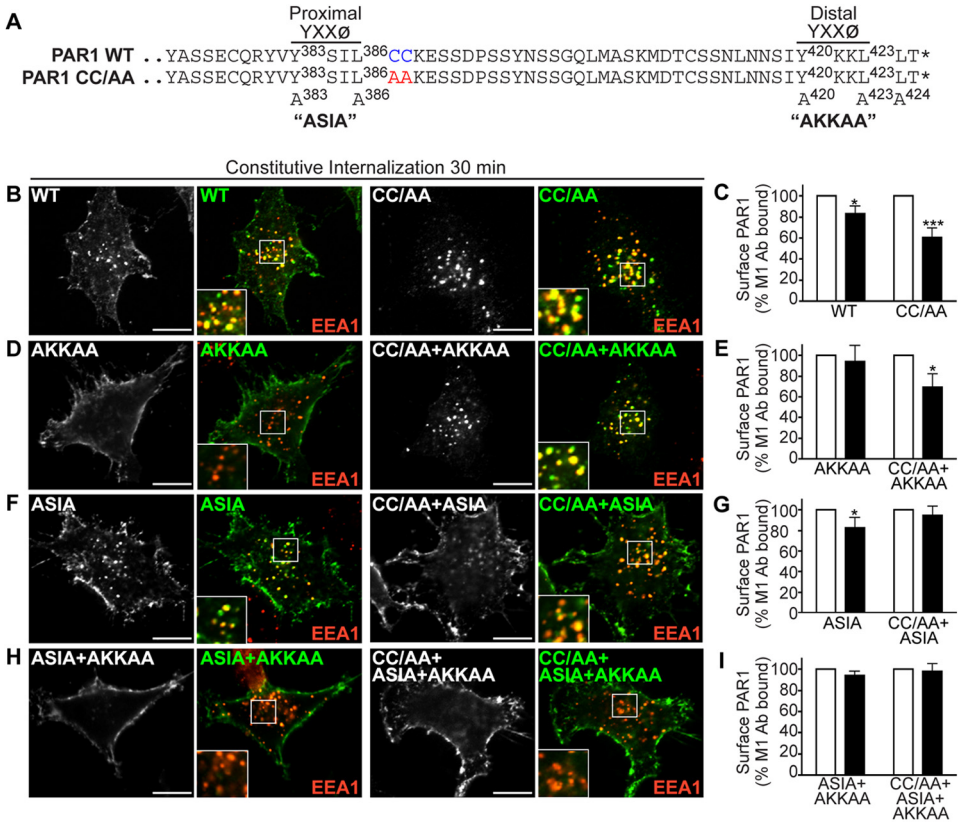

FIGURE 6. **Palmitoylation of PAR1 is important for proper utilization of C-tail tyrosine-based sorting motifs.** *A*, alignment of PAR1 WT and CC/AA mutant C-tail amino acid residues is shown. The PAR1 C-tail tyrosine-based *YXXØ* motifs are shown, and *superscript numbers* indicate the position of the critical tyrosine and leucine residues that were mutated to alanine to generate ASIA and AKKAA mutants. The *asterisk* indicates the end of the protein sequence. *B*, *D*, *F*, and *H*, HeLa cells expressing FLAG-PAR1 WT and mutants were prelabeled with polyclonal anti-FLAG antibody, washed, and incubated for 30 min at 37 °C. Cells were fixed, permeabilized, and co-stained for EEA1, a marker of early endosomes, and imaged by confocal microscopy. PAR1 (*green*) and EEA1 (*red*) colocalization is revealed by the *yellow color* in the merged images. *Insets* are magnifications of the *boxed areas*. Images are representative of many cells examined in multiple independent experiments. *Scale bar*, 10 μm. *C*, *E*, *G*, and *I*, HeLa cells expressing FLAG-PAR1 WT or mutants prelabeled with M1 anti-FLAG antibody were incubated for 30 min at 37 °C. Cells were fixed, and the amount of remaining receptor-bound antibody was quantified by ELISA. The data (mean ± S.D.; $n = 3$) shown are represented as the percent of initial M1 antibody bound derived from three separate experiments performed in triplicate. The differences in constitutive internalization of PAR1 WT and various mutants compared with the 0-min control were significant (*, $p < 0.05$) or (***, $p < 0.001$) as determined by two-way ANOVA and Bonferroni post-hoc tests.

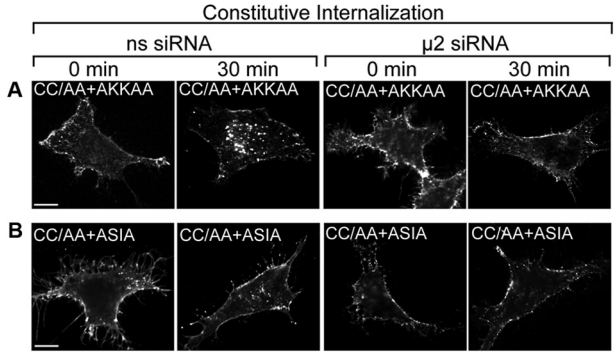

FIGURE 7. **AP-2 mediates constitutive internalization of PAR1 CC/AA+AKKAA and CC/AA+ASIA mutants.** HeLa cells were transfected with either FLAG-PAR1 CC/AA+AKKAA mutant (*A*) or PAR1 CC/AA+ASIA mutant (*B*) together with nonspecific (*ns*) siRNA or siRNA targeting the μ2-subunit of AP-2. Cells were prelabeled with polyclonal anti-FLAG antibody at 4 °C and then incubated 30 min at 37 °C. Cells were fixed, permeabilized, and immunostained for PAR1 and imaged by confocal microscopy. The images are representative of many cells examined in multiple independent experiments. *Scale bar*, 10 μm.

regulating tyrosine-based motif accessibility, we examined its function in PAR1 lysosomal degradation. We first compared the basal rate of FLAG-PAR1 WT and CC/AA mutant degradation in HeLa cells by quantifying the amount of receptor remaining at various times after incubation with cycloheximide, a protein synthesis inhibitor. In contrast to wild type receptor, the palmitoylation-deficient PAR1 mutant exhibited an enhanced rate of degradation with ~75% of receptor degraded at 180 min (Fig. 8, *B* and *D*) compared with ~25% degradation of wild type receptor (Fig. 8, *A* and *D*). To assess the contribution of the proximal tyrosine-based motif, we examined the degradation rate of the PAR1 CC/AA + ASIA mutant. Remarkably, mutation of the PAR1 CC/AA mutant proximal tyrosine motif restored basal turnover of the receptor that was comparable to wild type PAR1 (Fig. 8, *C* and *D*). We next examined PAR1 WT and mutant colocalization with LAMP1 to confirm that receptors are trafficked to lysosomes. PAR1 WT, CC/AA, and CC/AA+ASIA were incubated with anti-FLAG antibody for 1 h at 4 °C to prelabel the surface receptor cohort. Cells were then incubated for 30 min at 37 °C in media without agonist, and colocalization with LAMP1 was determined by confocal microscopy. PAR1 WT, CC/AA, and CC/AA +ASIA mutant exhibited colocalization with LAMP1 (Fig. 8, *E*–*G*). However, the extent of PAR1 CC/AA mutant colocalization with LAMP1 was greater compared with PAR1 WT and PAR1

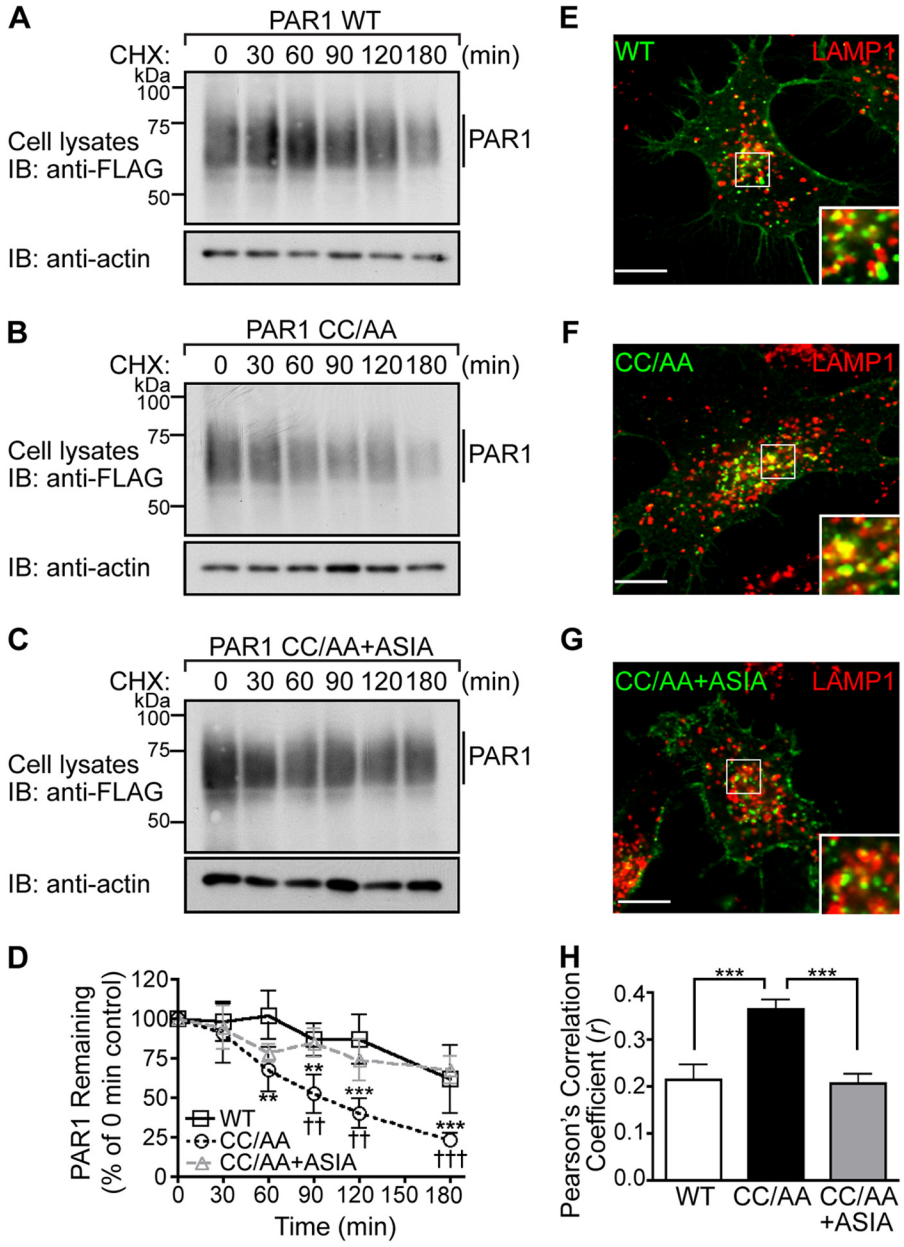

FIGURE 8. **The palmitoylation-deficient PAR1 mutant exhibits enhanced degradation.** *A–C*, HeLa cells expressing FLAG-PAR1 WT, CC/AA, or CC/AA+ASIA mutants were incubated in the presence of 10 μM cycloheximide (*CHX*) for various times at 37 °C. Cells were lysed, and equivalent amounts of cell lysates were immunoblotted (*IB*) with polyclonal anti-FLAG antibody to detect PAR1 expression. Membranes were stripped and reprobed for actin. *D*, PAR1 WT and mutant degradation was quantified (mean ± S.D.; $n = 3$) and is expressed as the percentage of remaining PAR1 compared with 0 min control. The difference in the amount of PAR1 WT *versus* CC/AA was statistically significant (**, $p < 0.01$; ***, $p < 0.001$) as determined by two-way ANOVA and Bonferroni post-hoc tests. The difference in the amount of PAR1 CC/AA *versus* PAR1 CC/AA+ASIA remaining was statistically significant (††, $p < 0.05$; †††, $p < 0.001$) as determined by two-way ANOVA with Bonferroni post-hoc tests. *E–G*, HeLa cells expressing FLAG-PAR1 WT, CC/AA, or CC/AA+ASIA mutant were prelabeled with anti-FLAG antibody on ice for 1 h in the presence of 2 mM leupeptin. Cells were then incubated for 30 min at 37 °C, fixed, permeabilized, and costained for LAMP1, a marker of late endosomes, and imaged by confocal microscopy. The images are representative of many cells examined from three independent experiments. *Scale bar*, 10 μm. PAR1 (*green*) and LAMP1 (*red*) colocalization is revealed by the *yellow color* in the merged images. *Insets* are magnifications of the *boxed areas*. *H*, colocalization of PAR1 and LAMP1 was quantified by determining Pearson's correlation coefficients from seven different cells. The difference in PAR1 CC/AA *versus* WT and CC/AA+ASIA colocalization with LAMP1 was statistically significant (***, $p < 0.001$) as determined by one-way ANOVA with a Tukey post-hoc test.

CC/AA + ASIA mutant as determined by Pearson's correlation coefficients (Fig. 8*H*). These findings suggest that palmitoylation regulates sorting of PAR1 from endosomes to lysosomes.

We next determined whether the enhanced rate of palmitoylation-deficient PAR1 mutant degradation resulted from increased internalization or enhanced sorting of internalized receptors from endosomes to lysosomes by directly examining degradation rates of internalized receptors. In these experiments the surface cohort of PAR1 WT or CC/AA mutant was labeled with biotin at 4 °C and either left on ice or warmed to 37 °C for 30 min to promote constitutive internalization. After PAR1 internalization, biotin remaining bound to the cell surface was removed, and cells were incubated for various times at 37 °C. Cells were then lysed, and the amount of internalized

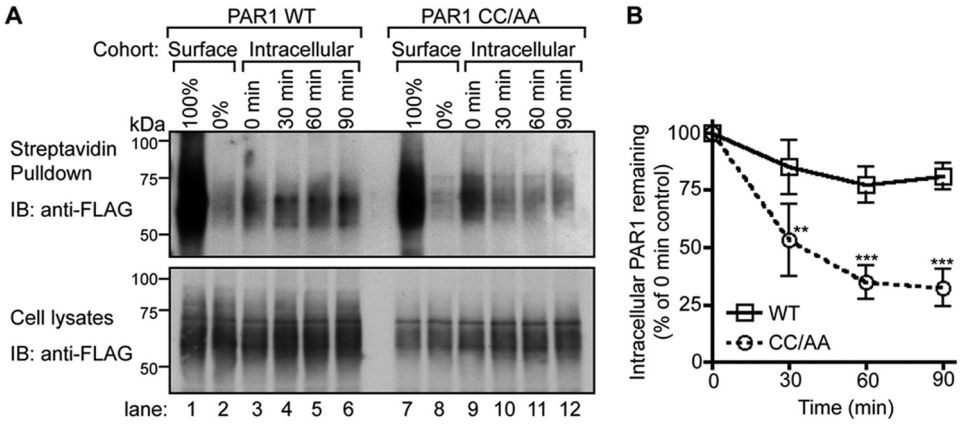

FIGURE 9. **Intracellular palmitoylation-deficient PAR1 exhibits enhanced degradation.** *A*, HeLa cells transfected with FLAG-PAR1 WT or CC/AA mutant were labeled with biotin at 4 °C. Cells were either left at 4 °C and represent the *Surface* cohort or warmed to 37 °C for 30 min and represent the *Intracellular* cohort. The biotin label was stripped from the Surface cohort as is shown as 0%. After 30 min of incubation, the remaining biotin label was then stripped from the Intracellular cohort cell surface before further incubation for 30, 60, or 90 min at 37 °C. Cells were lysed, and biotinylated proteins were isolated with streptavidin-conjugated agarose, resolved by SDS-PAGE, and immunoblotted (*IB*) with polyclonal anti-FLAG antibody to detect PAR1. An aliquot of total cell lysates was immunoblotted with polyclonal anti-FLAG antibody to control for PAR1 expression. *B*, the amount of intracellular PAR1 remaining from three independent experiments was quantified and normalized to receptor present in total cell lysates. Data (mean ± S.D.; $n = 3$) are expressed as a percentage of receptor remaining from the 0-min intracellular control. The difference in the amounts of internalized PAR1 CC/AA mutant remaining compared with WT at 30, 60, and 90 min was statistically significant (**, $p < 0.01$ and ***, $p < 0.001$) as determined by two-way ANOVA with a Bonferroni post-hoc test.

biotinylated PAR1 remaining was determined and represented as the "intracellular cohort." Both the surface cohort of PAR1 WT and CC/AA mutant exhibited substantial biotinylation, indicated as 100% (Fig. 9*A*, *lanes 1* and *7*), and subsequently biotin was efficiently removed from the surface cohort with glutathione, shown as 0% (Fig. 9*A*, *lanes 2* and *8*). In PAR1 WT- and CC/AA-expressing cells labeled with biotin, incubation for 30 min at 37 °C resulted in accumulation of intracellular receptor and is shown as the 0-min time point (Fig. 9*A*, *lanes 3* and *9*). In contrast to wild type PAR1, the internal pool of palmitoylation-deficient PAR1 CC/AA mutant displayed significant degradation after further incubation at 37 °C for 30, 60, and 90 min (Fig. 9, *A* and *B*, *lanes 4–6* and *10–12*). These data provide further evidence that palmitoylation of PAR1 is important for proper regulation of receptor lysosomal sorting.

To assess the function of AP-3 in PAR1 degradation, we used siRNA targeted against the δ-subunit of the AP-3 complex or nonspecific siRNA control and examined the rate of receptor degradation by immunoblotting. The loss of δ-adaptin expression results in degradation of other AP-3 components and disruption of AP-3 function (31). In nonspecific siRNA-transfected cells, PAR1 wild type displayed a modest level of basal turnover (Fig. 10, *A* and *C*, *lanes 1–3*) and was not significantly affected in cells deficient in δ-adaptin expression (Fig. 10, *A* and *C*, *lanes 4–6*). In contrast, palmitoylation-deficient PAR1 mutant displayed an enhanced rate of turnover that was virtually abolished in cells lacking δ-adaptin expression (Fig. 10, *B* and *D*). Taken together, these findings suggest that in the absence of palmitoylation, PAR1 exhibits enhanced lysosomal sorting that requires AP-3 function and an intact proximal tyrosine motif.

DISCUSSION

In the present study we demonstrate an essential function for palmitoylation in the proper regulation of PAR1 trafficking. We show that PAR1 is basally palmitoylated at highly conserved cysteine residues present in the C-tail domain. A palmitoylation-deficient PAR1 mutant is fully glycosylated, expressed on the cell surface, and competent to signal, indicating that palmitoylation is not required for biogenesis of a functional receptor. However, a palmitoylation-defective PAR1 mutant displayed enhanced constitutive internalization and an increased rate of lysosomal degradation. Moreover, AP-2 mediated enhanced internalization and interacted with the palmitoylation-deficient PAR1 mutant but through a different tyrosine motif compared with wild type receptor (10). The intracellular cohort of palmitoylation-deficient PAR1 also exhibited enhanced degradation, a process that required an intact tyrosine motif and AP-3. These findings suggest that palmitoylation of PAR1 is critical for proper adaptor protein recognition of tyrosine-based motifs and endocytic sorting. Thus, palmitoylation of PAR1 is critical for retaining appropriate receptor cell surface expression, which is essential for important biological processes such as hemostasis and thrombosis (32) and embryonic development (33, 34).

This study is the first to demonstrate palmitoylation of PAR1. The first GPCR shown to be palmitoylated was rhodopsin. An x-ray crystal structure of rhodopsin revealed the presence of palmitoyl groups covalently linked to juxtamembrane C-tail cysteine residues inserted into the lipid bilayer (21, 35). We found that palmitoylation of PAR1 also occurs at highly conserved Cys-387 and/or Cys-388 residues present in the C-tail domain, as mutation of these sites abrogated [^{3}H]palmitate incorporation. In addition to PAR1, several other GPCRs are palmitoylated at conserved juxtamembrane C-tail cysteines including the related PAR2 (36, 37). However, not all GPCRs are palmitoylated (38), and some GPCRs contain proximal as well as distal palmitoylation sites, suggesting that multiple intracellular loops may be formed within the C-tail domain of particular GPCRs (39, 40). Palmitoylation is a dynamic and reversible posttranslational modification that can be modu-

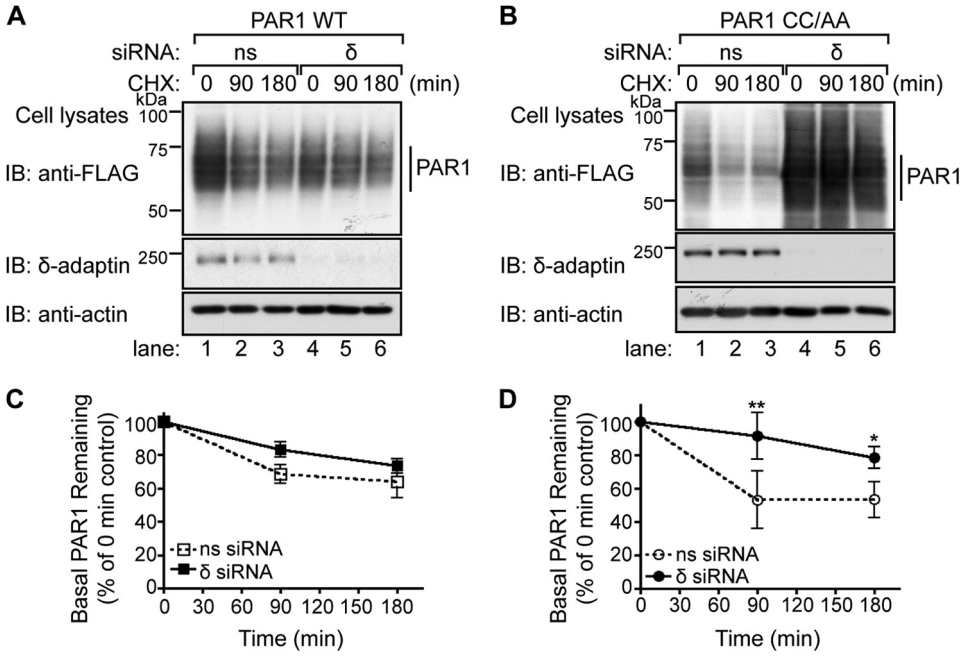

FIGURE 10. **Enhanced degradation of the palmitoylation-deficient PAR1 mutant is AP-3-dependent.** *A* and *B*, HeLa cells were transfected with FLAG-PAR1 WT or CC/AA and either nonspecific (*ns*) siRNA or siRNA targeted against the δ-subunit of AP-3. Cells were incubated in the presence of 10 μM cycloheximide (*CHX*) for 90 or 180 min at 37 °C and lysed, and equivalent amounts of cell lysates were immunoblotted (*IB*) with polyclonal anti-FLAG antibody to detect PAR1. Membranes were stripped and reprobed with anti-δ-adaptin and anti-actin antibodies. *C* and *D*, PAR1 WT and CC/AA degradation were quantified from three individual experiments. Data (mean ± S.D.; $n = 3$) are expressed as a percent of total receptor remaining relative to the 0 min control. PAR1 CC/AA mutant degradation was significantly attenuated in δ-siRNA-transfected cells compared with nonspecific siRNA-treated control cells (**, $p < 0.01$ and *, $p < 0.05$) as determined by two-way ANOVA with a Bonferroni post-hoc test.

lated. An increase in palmitoylation of the β2-adrenergic receptor (41) and other GPCRs (18) was observed after agonist stimulation, indicating that receptor palmitoylation is a regulated process. However, the thromboxane A2 receptor TPα isoform (38) and the 5-HT1A serotonin receptor (42) appear to be palmitoylated constitutively and not affected by agonist stimulation. Although we failed to observe any change in [^{3}H]palmitate incorporation after agonist activation of PAR1 expressed in HeLa cells or endogenous PAR1 expressed natively in endothelial cells, we cannot exclude the possibility that PAR1 is modified dynamically by palmitoylation and de-palmitoylation at steady state, as it would not be evident under the metabolic labeling conditions employed in our studies.

Palmitoylation serves distinct functions for different receptor types; however, the role of palmitoylation in regulation of PAR1 signaling or trafficking has not been previously investigated. We found that palmitoylation of PAR1 is critical for regulating appropriate adaptor protein interaction with C-tail tyrosine motifs and sorting through the endocytic pathway and has a modest affect on receptor-G protein coupling. Tyrosine-based motifs can function as signals for endocytosis or lysosomal sorting depending on their position relative to the plasma membrane (11, 43). PAR1 contains two tyrosine-based motifs within the C-tail domain that appear to have distinct functions. The distal tyrosine motif is recognized by AP-2 and mediates PAR1 constitutive internalization (6, 10). Intriguingly, however, in the absence of PAR1 palmitoylation, AP-2 mediates receptor constitutive internalization via the proximal tyrosine motif rather than the distal motif. Similar to PAR1, the thromboxane A2 receptor TPβ isoform harbors a C-tail $YX_3Ø$ motif that functions in constitutive internalization (44). Interestingly, TPβ is constitutively palmitoylated at multiple C-tail cysteine residues, yet the $YX_3Ø$ motif resides near the most proximal palmitoylated cysteine (38). Perturbation of TPβ palmitoylation by mutation of the distal cysteine residues resulted in loss of constitutive internalization (38), suggesting that palmitoylation is important for the function of tyrosine motifs and constitutive internalization. This suggests that the secondary structure created by receptor palmitoylation is important for proper engagement of AP-2 with sorting motifs. In addition to PAR1 and TPβ receptor, ~30 other mammalian GPCRs harbor canonical tyrosine-based motifs within their C-tail domain (45), and in some cases nearby cysteine residues are known to be palmitoylated (46–52). Thus, GPCR palmitoylation may have a broad function in regulating adaptor protein interaction with sorting signals and is likely to be important for maintaining appropriate expression of receptors on the cell surface.

AP-2 coordinates cargo recruitment and clathrin-coated pit formation at the plasma membrane, whereas AP-3 functions mainly at the sorting endosome to facilitate lysosomal transport (11). In recent work we discovered that AP-3 regulated lysosomal degradation of activated PAR1 through interaction with a C-tail proximal tyrosine motif YSIL at the sorting endosome to facilitate degradation (16). In the present study we have determined that AP-3-mediated lysosomal sorting of PAR1 is regulated by palmitoylation. We found that palmitoylation-deficient PAR1 mutant exhibits enhanced degradation that is ablated in cells lacking AP-3. These findings suggest an important function for palmitoylation of PAR1 in regulation of AP-3

binding and sorting at endosomes. The yeast casein kinase Yck3p resides at the limiting membrane of the vacuole, an organelle equivalent to the mammalian lysosome, and requires both palmitoylation at its C terminus and AP-3 binding to a canonical tyrosine *YXXØ* motif for proper sorting to the vacuole (53).

In addition to trafficking, PAR1 palmitoylation modulates receptor-G protein coupling, a phenotype that was previously observed with a PAR1 CC/SS mutant (28). Intriguingly, a small molecule inhibitor JF5 blocked PAR1 activation of G_q signaling in platelets and thrombus formation *in vivo* but had no affect on G_{12} signaling in Madin-Darby canine kidney cells (54). The inhibitory activity of JF5 required the PAR1 putative eighth helix formed by palmitoylation and was not specific to PAR1, as signaling by the chemokine CCR4 and serotonin 5-$HT2_A$ receptors containing cysteine residues and a putative eighth helix were similarly inhibited (54). Thus, palmitoylation of certain GPCRs appears to generate an intracytosolic interface that can be targeted for therapeutic development. These findings highlight the importance of identifying the machinery responsible for GPCR palmitoylation as well as the function of palmitoylation for GPCRs deemed to be important targets for drug development.

Our study provides the first molecular insight into the mechanism by which palmitoylation of a GPCR regulates adaptor protein recognition of sorting signals. We propose that palmitoylation of PAR1 has an essential function that is important for maintaining appropriate receptor surface expression by limiting accessibility of AP-2 at the plasma membrane and AP-3 at the sorting endosome. Given the critical role of PAR1 in hemostasis, thrombosis, and embryonic development (34), we speculate that a major defect resulting in complete loss of palmitoylation would be detrimental. However, it remains unclear if PAR1 palmitoylation is dynamically regulated at subcellular organelles and/or whether de-palmitoylation of PAR1 ever occurs naturally.

Acknowledgments—We thank members of the Trejo laboratory for constructs, comments, and advice.

REFERENCES

1. Soh, U. J., Dores, M. R., Chen, B., and Trejo, J. (2010) Signal transduction by protease-activated receptors. *Br. J. Pharmacol.* **160,** 191–203
2. Vu, T. K., Wheaton, V. I., Hung, D. T., Charo, I., and Coughlin, S. R. (1991) Domains specifying thrombin-receptor interaction. *Nature* **353,** 674–677
3. Coughlin, S. R. (2005) Protease-activated receptors in hemostasis, thrombosis and vascular biology. *J. Thromb. Haemost.* **3,** 1800–1814
4. Vu, T. K., Hung, D. T., Wheaton, V. I., and Coughlin, S. R. (1991) Molecular cloning of a functional thrombin receptor reveals a novel proteolytic mechanism of receptor activation. *Cell* **64,** 1057–1068
5. Chen, J., Ishii, M., Wang, L., Ishii, K., and Coughlin, S. R. (1994) Thrombin receptor activation. Confirmation of the intramolecular tethered liganding hypothesis and discovery of an alternative intermolecular liganding mode. *J. Biol. Chem.* **269,** 16041–16045
6. Paing, M. M., Stutts, A. B., Kohout, T. A., Lefkowitz, R. J., and Trejo, J. (2002) β-Arrestins regulate protease-activated receptor-1 desensitization but not internalization or Down-regulation. *J. Biol. Chem.* **277,** 1292–1300
7. Chen, C. H., Paing, M. M., and Trejo, J. (2004) Termination of protease-activated receptor-1 signaling by β-arrestins is independent of receptor phosphorylation. *J. Biol. Chem.* **279,** 10020–10031
8. Arora, P., Ricks, T. K., and Trejo, J. (2007) Protease-activated receptor signalling, endocytic sorting, and dysregulation in cancer. *J. Cell Sci.* **120,** 921–928
9. Booden, M. A., Eckert, L. B., Der, C. J., and Trejo, J. (2004) Persistent signaling by dysregulated thrombin receptor trafficking promotes breast carcinoma cell invasion. *Mol. Cell. Biol.* **24,** 1990–1999
10. Paing, M. M., Johnston, C. A., Siderovski, D. P., and Trejo, J. (2006) Clathrin adaptor AP2 regulates thrombin receptor constitutive internalization and endothelial cell resensitization. *Mol. Cell. Biol.* **26,** 3231–3242
11. Bonifacino, J. S., and Traub, L. M. (2003) Signals for sorting of transmembrane proteins to endosomes and lysosomes. *Annu. Rev. Biochem.* **72,** 395–447
12. Ohno, H., Stewart, J., Fournier, M. C., Bosshart, H., Rhee, I., Miyatake, S., Saito, T., Gallusser, A., Kirchhausen, T., and Bonifacino, J. S. (1995) Interaction of tyrosine-based sorting signals with clathrin-associated proteins. *Science* **269,** 1872–1875
13. Hein, L., Ishii, K., Coughlin, S. R., and Kobilka, B. K. (1994) Intracellular targeting and trafficking of thrombin receptors. A novel mechanism for resensitization of a G protein-coupled receptor. *J. Biol. Chem.* **269,** 27719–27726
14. Trejo, J., Hammes, S. R., and Coughlin, S. R. (1998) Termination of signaling by protease-activated receptor-1 is linked to lysosomal sorting. *Proc. Natl. Acad. Sci. U.S.A.* **95,** 13698–13702
15. Chen, B., Dores, M. R., Grimsey, N., Canto, I., Barker, B. L., and Trejo, J. (2011) Adaptor protein complex-2 (AP-2) and epsin-1 mediate protease-activated receptor-1 internalization via phosphorylation- and ubiquitination-dependent sorting signals. *J. Biol. Chem.* **286,** 40760–40770
16. Dores, M. R., Paing, M. M., Lin, H., Montagne, W. A., Marchese, A., and Trejo, J. (2012) AP-3 regulates PAR1 ubiquitin-independent MVB/lysosomal sorting via an ALIX-mediated pathway. *Mol. Biol. Cell* **23,** 3612–3623
17. Dores, M. R., Chen, B., Lin, H., Soh, U. J., Paing, M. M., Montagne, W. A., Meerloo, T., and Trejo, J. (2012) ALIX binds a YPX(3)L motif of the GPCR PAR1 and mediates ubiquitin-independent ESCRT-III/MVB sorting. *J. Cell Biol.* **197,** 407–419
18. Chini, B., and Parenti, M. (2009) G-protein-coupled receptors, cholesterol, and palmitoylation. Facts about fats. *J. Mol. Endocrinol.* **42,** 371–379
19. Linder, M. E., and Deschenes, R. J. (2007) Palmitoylation. Policing protein stability and traffic. *Nat. Rev. Mol. Cell Biol.* **8,** 74–84
20. Iwanaga, T., Tsutsumi, R., Noritake, J., Fukata, Y., and Fukata, M. (2009) Dynamic protein palmitoylation in cellular signaling. *Prog. Lipid Res.* **48,** 117–127
21. Palczewski, K., Kumasaka, T., Hori, T., Behnke, C. A., Motoshima, H., Fox, B. A., Le Trong, I., Teller, D. C., Okada, T., Stenkamp, R. E., Yamamoto, M., and Miyano, M. (2000) Crystal structure of rhodopsin. A G protein-coupled receptor. *Science* **289,** 739–745
22. Trejo, J., Altschuler, Y., Fu, H. W., Mostov, K. E., and Coughlin, S. R. (2000) Protease-activated receptor-1 down-regulation. A mutant HeLa cell line suggests novel requirements for PAR1 phosphorylation and recruitment to clathrin-coated pits. *J. Biol. Chem.* **275,** 31255–31265
23. Edgell, C. J., McDonald, C. C., and Graham, J. B. (1983) Permanent cell line expressing human factor VIII-related antigen established by hybridization. *Proc. Natl. Acad. Sci. U.S.A.* **80,** 3734–3737
24. Dunn, K. W., Kamocka, M. M., and McDonald, J. H. (2011) A practical guide to evaluating colocalization in biological microscopy. *Am. J. Physiol. Cell Physiol.* **300,** C723–C742
25. Shapiro, M. J., Trejo, J., Zeng, D., and Coughlin, S. R. (1996) Role of the thrombin receptor's cytoplasmic tail in intracellular trafficking. Distinct determinants for agonist-triggered versus tonic internalization and intracellular localization. *J. Biol. Chem.* **271,** 32874–32880
26. Wolfe, B. L., Marchese, A., and Trejo, J. (2007) Ubiquitination differentially regulates clathrin-dependent internalization of protease-activated receptor-1. *J. Cell Biol.* **177,** 905–916
27. Soto, A. G., and Trejo, J. (2010) *N*-Linked glycosylation of protease-activated receptor-1 second extracellular loop. A critical determinant for ligand-induced receptor activation and internalization. *J. Biol. Chem.* **285,** 18781–18793

28. Swift, S., Leger, A. J., Talavera, J., Zhang, L., Bohm, A., and Kuliopulos, A. (2006) Role of the PAR1 receptor 8th helix in signaling. The 7–8-1 receptor activation mechanism. *J. Biol. Chem.* **281,** 4109–4116
29. Coughlin, S. R. (2000) Thrombin signalling and protease-activated receptors. *Nature* **407,** 258–264
30. Taylor, S. J., Chae, H. Z., Rhee, S. G., and Exton, J. H. (1991) Activation of the β 1 isozyme of phospholipase C by α subunits of the Gq class of G proteins. *Nature* **350,** 516–518
31. Peden, A. A., Rudge, R. E., Lui, W. W., and Robinson, M. S. (2002) Assembly and function of AP-3 complexes in cells expressing mutant subunits. *J. Cell Biol.* **156,** 327–336
32. Kahn, M. L., Nakanishi-Matsui, M., Shapiro, M. J., Ishihara, H., and Coughlin, S. R. (1999) Protease-activated receptors 1 and 4 mediate activation of human platelets by thrombin. *J. Clin. Invest.* **103,** 879–887
33. Connolly, A. J., Ishihara, H., Kahn, M. L., Farese, R. V., Jr., and Coughlin, S. R. (1996) Role of the thrombin receptor in development and evidence for a second receptor. *Nature* **381,** 516–519
34. Griffin, C. T., Srinivasan, Y., Zheng, Y. W., Huang, W., and Coughlin, S. R. (2001) A role for thrombin receptor signaling in endothelial cells during embryonic development. *Science* **293,** 1666–1670
35. Ovchinnikov, Y. u. A., Abdulaev, N. G., and Bogachuk, A. S. (1988) Two adjacent cysteine residues in the C-terminal cytoplasmic fragment of bovine rhodopsin are palmitylated. *FEBS Lett.* **230,** 1–5
36. Adams, M. N., Christensen, M. E., He, Y., Waterhouse, N. J., and Hooper, J. D. (2011) The role of palmitoylation in signalling, cellular trafficking, and plasma membrane localization of protease-activated receptor-2. *PLoS One* **6,** e28018
37. Botham, A., Guo, X., Xiao, Y. P., Morice, A. H., Compton, S. J., and Sadofsky, L. R. (2011) Palmitoylation of human proteinase-activated receptor-2 differentially regulates receptor-triggered ERK1/2 activation, calcium signaling, and endocytosis. *Biochem. J.* **438,** 359–367
38. Reid, H. M., and Kinsella, B. T. (2007) Palmitoylation of the TPβ isoform of the human thromboxane A2 receptor. Modulation of G protein. Effector coupling and modes of receptor internalization. *Cell Signal* **19,** 1056–1070
39. Zuckerman, D. M., Hicks, S. W., Charron, G., Hang, H. C., and Machamer, C. E. (2011) Differential regulation of two palmitoylation sites in the cytoplasmic tail of the β1-adrenergic receptor. *J. Biol. Chem.* **286,** 19014–19023
40. Ponimaskin, E. G., Heine, M., Joubert, L., Sebben, M., Bickmeyer, U., Richter, D. W., and Dumuis, A. (2002) The 5-hydroxytryptamine(4a) receptor is palmitoylated at two different sites, and acylation is critically involved in regulation of receptor constitutive activity. *J. Biol. Chem.* **277,** 2534–2546
41. Moffett, S., Mouillac, B., Bonin, H., and Bouvier, M. (1993) Altered phosphorylation and desensitization patterns of a human β 2-adrenergic receptor lacking the palmitoylated Cys341. *EMBO J.* **12,** 349–356
42. Papoucheva, E., Dumuis, A., Sebben, M., Richter, D. W., and Ponimaskin, E. G. (2004) The 5-hydroxytryptamine(1A) receptor is stably palmitoylated, and acylation is critical for communication of receptor with G_i protein. *J. Biol. Chem.* **279,** 3280–3291
43. Rohrer, J., Schweizer, A., Russell, D., and Kornfeld, S. (1996) The targeting of Lamp1 to lysosomes is dependent on the spacing of its cytoplasmic tail tyrosine sorting motif relative to the membrane. *J. Cell Biol.* **132,** 565–576
44. Parent, J. L., Labrecque, P., Driss Rochdi, M., and Benovic, J. L. (2001) Role of the differentially spliced carboxyl terminus in thromboxane A2 receptor trafficking. Identification of a distinct motif for tonic internalization. *J. Biol. Chem.* **276,** 7079–7085
45. Marchese, A., Paing, M. M., Temple, B. R., and Trejo, J. (2008) G protein-coupled receptor sorting to endosomes and lysosomes. *Annu. Rev. Pharmacol. Toxicol.* **48,** 601–629
46. Percherancier, Y., Planchenault, T., Valenzuela-Fernandez, A., Virelizier, J. L., Arenzana-Seisdedos, F., and Bachelerie, F. (2001) Palmitoylation-dependent control of degradation, life span, and membrane expression of the CCR5 receptor. *J. Biol. Chem.* **276,** 31936–31944
47. Pizard, A., Blaukat, A., Michineau, S., Dikic, I., Müller-Esterl, W., Alhenc-Gelas, F., and Rajerison, R. M. (2001) Palmitoylation of the human bradykinin B2 receptor influences ligand efficacy. *Biochemistry* **40,** 15743–15751
48. Hayashi, M. K., and Haga, T. (1997) Palmitoylation of muscarinic acetylcholine receptor m2 subtypes. Reduction in their ability to activate G proteins by mutation of a putative palmitoylation site, cysteine 457, in the carboxyl-terminal tail. *Arch. Biochem. Biophys.* **340,** 376–382
49. Fukushima, Y., Saitoh, T., Anai, M., Ogihara, T., Inukai, K., Funaki, M., Sakoda, H., Onishi, Y., Ono, H., Fujishiro, M., Ishikawa, T., Takata, K., Nagai, R., Omata, M., and Asano, T. (2001) Palmitoylation of the canine histamine H2 receptor occurs at Cys-305 and is important for cell surface targeting. *Biochim. Biophys. Acta* **1539,** 181–191
50. Kvachnina, E., Dumuis, A., Wlodarczyk, J., Renner, U., Cochet, M., Richter, D. W., and Ponimaskin, E. (2009) Constitutive Gs-mediated, but not G12-mediated, activity of the 5-hydroxytryptamine 5-HT7(a) receptor is modulated by the palmitoylation of its C-terminal domain. *Biochim. Biophys. Acta* **1793,** 1646–1655
51. Okamoto, Y., Ninomiya, H., Tanioka, M., Sakamoto, A., Miwa, S., and Masaki, T. (1997) Palmitoylation of human endothelinB. Its critical role in G protein coupling and a differential requirement for the cytoplasmic tail by G protein subtypes. *J. Biol. Chem.* **272,** 21589–21596
52. Holliday, N. D., and Cox, H. M. (2003) Control of signalling efficacy by palmitoylation of the rat Y1 receptor. *Br. J. Pharmacol.* **139,** 501–512
53. Sun, B., Chen, L., Cao, W., Roth, A. F., and Davis, N. G. (2004) The yeast casein kinase Yck3p is palmitoylated, then sorted to the vacuolar membrane with AP-3-dependent recognition of a $YXX\phi$ adaptin sorting signal. *Mol. Biol. Cell* **15,** 1397–1406
54. Dowal, L., Sim, D. S., Dilks, J. R., Blair, P., Beaudry, S., Denker, B. M., Koukos, G., Kuliopulos, A., and Flaumenhaft, R. (2011) Identification of an antithrombotic allosteric modulator that acts through helix 8 of PAR1. *Proc. Natl. Acad. Sci. U.S.A.* **108,** 2951–2956